



Inverse eigenvalue sensing with corner coupled square plate MEMS resonators array

Guowei Tao¹ · Bhaskar Choubey¹

Received: 4 January 2018 / Revised: 2 March 2018 / Accepted: 6 March 2018 / Published online: 13 March 2018
© The Author(s) 2018

Abstract

Monitoring the collective behaviour of coupled micro/nano resonators array provides a distinct opportunity for high resolution multi-function sensing. We report an inverse eigenvalue analysis based sensing approach for large array of coupled micro/nano resonators. A new characterization algorithm is proposed to precisely extract the system matrix of those multiplexed sensors with reduced algorithmic complexity and below 1% relative error. The method has been verified experimentally using five corner coupled square plate MEMS resonators with a natural frequency close to 0.85 MHz. The method is also capable of characterizing the fabrication process and important sensor parameters such as the spring constant and coupling ratio.

Keywords MEMS sensor readout · Coupled resonators array · Inverse eigenvalue analysis · Process variability

1 Introduction

Micro/nano resonator has been widely implemented as inertial sensors for mass, force and acceleration sensing applications [1–4]. Coupled resonators have been suggested to improve the sensitivity and functionality of those sensors. There are several advantages of mechanically or electrically coupling them together. First, the mode localisation effect opens up new sensing methods, such as multi-mode sensing and the use of eigenvector (amplitude), to push down the limit by several orders of magnitude [5–8]. Second, it is possible to drive and readout from only one single resonator to find all eigenvalues (resonance frequencies) of a large array thanks to the collective behaviour [9]. This reduces the actuation complexity and turns the system into a single-input-single-output (SISO) multiplexed sensors array. In addition, coupling facilitates the characterization of large resonators array utilizing an inverse eigenvalue analysis (IEA) method. By perturbing the terminal element of a coupled array, two unique sets of eigenvalues are recorded to extract the system matrix using

inverse problem theory. The system matrix is associated with important device properties such as Young's modulus [10], mass sensitivity [11] and process variability [12]. However, existing IEA techniques require solving complicated eigenvectors or orthogonal polynomials, and hence become complicated when the array size is large.

Herein, we present a simplified IEA technique to circumvent this issue, thereby providing a new solution to system matrix determination. An array of five nearest-neighbour coupled square plate resonators were fabricated via the multi-user MEMS processes (MUMPs) to validate the ideas. Using the new IEA method, important sensor information including sensitivity and coupling ratio can be provided, which are of substantial interest for resonator designers.

The article is organised as follows: Section 2 provides the mathematical foundation of the simplified IEA technique to extract eigenvectors and system matrix, and analyses its complexity and accuracy. Section 3 describes the MEMS square plate resonator used in this research, including the fabrication process, electromechanical properties, experimental setup and result of a prototype sensor. Section 4 studies the collective behaviour of coupled systems using an example of five coupled resonators. Section 5 characterizes the sensor using perturbation analysis and the proposed IEA technique. System matrix and other

✉ Guowei Tao
guowei.tao@eng.ox.ac.uk

¹ Department of Engineering Science, University of Oxford, Oxford OX1 3PJ, UK

parameters such as spring constant and coupling ratio are therefore determined. Section 6 gives the conclusion.

2 Inverse eigenvalue analysis

2.1 Coupled systems

An array of n nearest-neighbour coupled resonators can be modelled by the following equation

$$\mathbf{M}\ddot{\mathbf{v}} + \mathbf{B}\dot{\mathbf{v}} + \mathbf{K}\mathbf{v} = \mathbf{F} \tag{1}$$

where \mathbf{M} , \mathbf{B} and \mathbf{K} are mass, damping and stiffness matrix. \mathbf{v} and \mathbf{F} are two column vectors representing the displacement and driving force of each element. For low damping, the equation transforms into the classic eigenvalue problem

$$\mathbf{S}\mathbf{x}_i = \lambda_i\mathbf{x}_i \tag{2}$$

where $\mathbf{S} = \mathbf{M}^{-1/2}\mathbf{K}\mathbf{M}^{1/2}$ is the symmetric tridiagonal (Jacobian) system matrix. At the i th mode, \mathbf{S} has eigenvalues $\lambda_i = \omega_i^2$ and eigenvectors \mathbf{x}_i that are related to resonance frequencies and amplitudes. Ideally, there are n eigenvalues already available from the n resonance peaks, which can be observed from any element of the array due to collective behaviour. A mass or stiffness perturbation upon one resonator would lead to another set of n unique eigenvalues λ_i^* .

2.2 New characterization algorithm

With the two sets of readily available eigenvalues before and after perturbation, the previous Choubey’s algorithm can be used to reconstruct the system matrix [13]. This method, however, requires numerous multiplication and division operators to derive all eigenvectors. It is computationally expensive and impractical for real-world sensing when the array size n becomes large. The algorithm can be linearised by ignoring high order terms while preserving adequate precision. When a perturbation happens on the p th element, the new system matrix becomes

$$\mathbf{S}^* = \mathbf{S} + \Delta\mathbf{S} \tag{3}$$

where $\Delta\mathbf{S}$ is a matrix filled with zeros except for the (p, p) th entry $\Delta S_{p,p}$, which can be calculated using the trace property of the system matrix before and after perturbation

$$\Delta S_{p,p} = \sum_{i=1}^n \lambda_i^* - \sum_{i=1}^n \lambda_i = \sum_{i=1}^n \Delta\lambda_i \tag{4}$$

The eigenvalue problem has been updated to

$$(\mathbf{S} + \Delta\mathbf{S})(\mathbf{x}_i + \Delta\mathbf{x}_i) = (\lambda_i + \Delta\lambda_i)(\mathbf{x}_i + \Delta\mathbf{x}_i) \tag{5}$$

Since $\mathbf{x}_i^T \mathbf{x}_i = 1$ and $\mathbf{x}_i^T \mathbf{S} = \mathbf{x}_i^T \lambda_i$, ignoring high order terms yields

$$\mathbf{x}_i^T \Delta\mathbf{S}\mathbf{x}_i = \Delta\lambda_i \tag{6}$$

which leads to a simple solution

$$x_{p,i}^2 = \frac{\Delta\lambda_i}{\Delta S_{p,p}} \tag{7}$$

This can be compared with the previous approach [13]

$$x_{p,i}^2 = \frac{\Delta\lambda_i}{\Delta S_{p,p}} \prod_{j=1, j \neq i}^n \frac{\lambda_i - \lambda_j^*}{\lambda_i - \lambda_j} \tag{8}$$

2.3 Complexity and accuracy

Figure 1 shows the algorithmic complexity of the new method and the previous Choubey’s approach for different number of resonators using MATLAB computation time analysis. The new method has reduced the complexity from $O(n^2)$ to $O(n)$, which facilitates signal processing requirement and paves the way for rapid characterization of massive sensors array. With the amplitudes of the p th resonator known for all modes, the (p, p) th element of the system matrix is determined by

$$S_{p,p} = (x_{p,1} \quad \dots \quad x_{p,n}) \begin{pmatrix} \lambda_1 & & \\ & \ddots & \\ & & \lambda_n \end{pmatrix} \begin{pmatrix} x_{p,1} \\ \vdots \\ x_{p,n} \end{pmatrix} \tag{9}$$

When perturbation happens on the terminal element ($p = 1$ or $p = n$), inverse Lanczos’ algorithm can be applied to extract all other entries in the system matrix

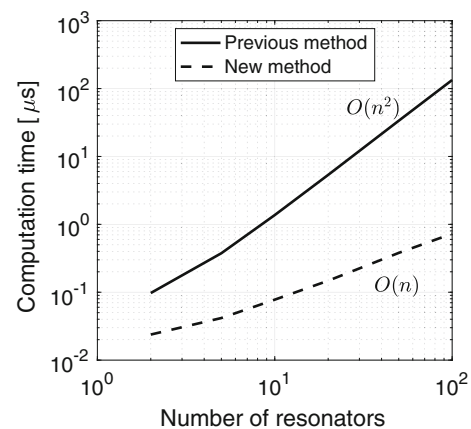


Fig. 1 Algorithmic complexity of the new and previous method using MATLAB computation time

iteratively [14, 15]. Hence all mass normalised stiffnesses and coupling strengths have been determined by simply recording the two sets of eigenvalues from any element.

To appreciate the accuracy of the new method for system matrix extraction, the mean absolute error of diagonal elements and off-diagonal elements are depicted in Fig. 2 using a simulated array of five coupled resonators. Perturbation applied to the terminal element, hence inverse Lanczos’ algorithm was used to determine the full system matrix. Various perturbation levels and coupling strengths were considered. Results suggest that for small perturbation ($\Delta S_{p,p}/S_{p,p} < k_c/k$), the relative error can be well controlled below 1%. It is worth noting that off-diagonal elements, which correspond to coupling spring constants, are more prone to error, particularly for a weaker coupling. For weak coupling, these spring constants are very small compared with diagonal elements, hence more sensitive to numerical error. In practice, diagonal elements are of more importance as they contain mass and stiffness for individual resonators.

3 Square plate resonator

3.1 Device architecture and fabrication process

Square plate resonator is a simple structure that utilises the transverse mode vibration of a centre-stemmed square

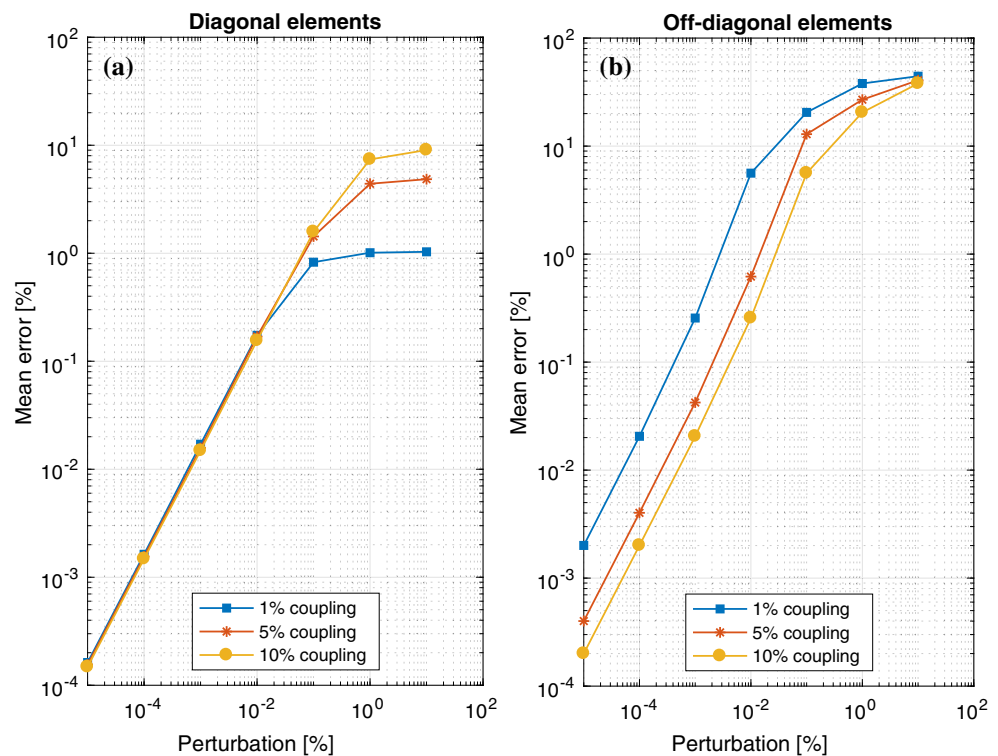
membrane, and has already been applied in the fields of radio frequency and communication [16]. The design benefits from high quality factor Q , low impedance and convenient eigenvalue readout channel, which can be potentially used as sensors or transducers.

The device was designed and fabricated through the PolyMUMPs programme provided by the MEMSCAP. The fabrication typically involves a three-layer polysilicon surface micromachining process [17]. Two layers of polysilicon, i.e. Poly 1 and Poly 2, were used in our design, as shown in Fig. 3(a). These polysilicon layers are conductive with 10–20 sheet resistance. Poly 1 shaped the driving and readout electrodes as well as interconnections at the bottom. Poly 2 acted as the centre-stemmed square plate membrane. The thickness t of the square plate ($t = 1.5 \mu\text{m}$) and the gap distance g between the top plate and bottom electrode ($g = 0.75 \mu\text{m}$) were defined by the process. As Poly 0 layer was not used in our design, the device was anchored to the Nitride substrate by filling an anchor hole with Poly 1. The hole was formed by patterning silicon dioxide with a mask layer and reactive ion etching (RIE).

3.2 Electromechanical properties

The natural frequency f_0 of such square plate membrane with Young’s modulus E and density ρ is given by [18]

Fig. 2 Accuracy of the new method for extracting **a** diagonal elements and **b** off-diagonal elements



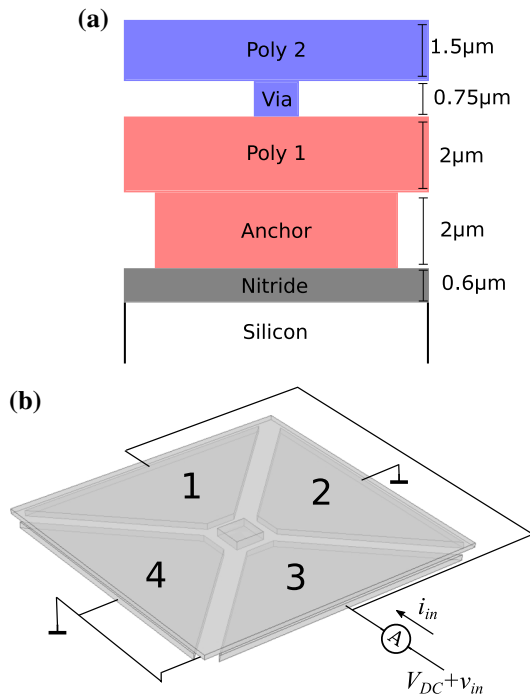


Fig. 3 **a** Cross-section view of the PolyMUMPs layers used for device fabrication and **b** electrical connection for one resonator

$$f_0 = 0.9697 \sqrt{\frac{E t}{\rho L^2}} \approx \sqrt{\frac{E t}{\rho L^2}} \tag{10}$$

The side length L is designed to be $100 \mu\text{m}$ to provide around 1.2 MHz resonance. The mass and stiffness of the resonator are calculated by

$$m = \rho t L^2 \tag{11}$$

and

$$k = E \left(\frac{2\pi}{L} \right)^2 t^3 \tag{12}$$

Hence the designed mass and stiffness for each resonator are 34 ng and 2020 N/m . Figure 3(b) depicts the electrical circuit for the sensor. The device implements a direct drive and readout scheme. A DC bias V_{DC} superimposed with a small AC signal v_{in} is applied to electrode 1 and 3. Electrode 2, 4 and the top plate are grounded. Change in resonance magnitude results in an AC current i_{in} which is linearly dependent on the vibration velocity [19]. The conductance is calculated by [16]

$$|Y| = \left| \frac{i_{in}}{v_{in}} \right| = \frac{Q \varepsilon^2 A_{eff}^2 V_{DC}^2}{\sqrt{k m g^4}} \tag{13}$$

with ε being the permittivity and A_{eff} the effective area where top plate and driving electrodes overlap. The typical

conductance of each resonator, assuming $Q = 10^4$ and $V_{DC} = 10 \text{ V}$, is estimated to be $14.5 \mu\text{S}$.

A large DC bias voltage is preferred for strong signal amplitude; however, may cause non-linear and pull-in effect that can potentially destroy the device. Figure 4 shows the static displacement of the membrane under different bias voltages using COMSOL finite element method (FEM) simulation. The pull-in voltage is projected to be 50 V . The spring constant of the resonator can be tuned by tweaking the DC voltage, hence introducing a negative electrostatic stiffness k_E [13]

$$k_E = -\frac{\varepsilon A_{eff}}{g^3} V_{DC}^2 \tag{14}$$

that reduces the resonance frequency. Such spring softening effect provides a flexible way of perturbing the resonator as required by the IEA.

3.3 Single resonator

The SEM image of a single resonator is illustrated in Fig. 5. An impedance analyser with frequency sweep functionality (Hioki IM3570) supplies the required test voltages and measures the impedance or conductance with below 0.08% error. Each frequency sweep takes less than 1 ms by recording up to 800 frequency points.

Figure 6 shows the conductance and phase response of a prototype sensor by applying $V_{DC} = 10 \text{ V}$ and $v_{in} = 50 \text{ mV}$ under a low pressure level $P < 100 \text{ mPa}$. Fabricated resonators demonstrate a natural frequency between 0.8 and 0.85 MHz , which is approximately 30% less than the nominal frequency 1.2 MHz due to fabrication tolerance. This was likely to be caused by the extra side length when depositing Poly 2 layer onto the uneven silicon dioxide formed during the patterning process, thereby increasing the effective length by approximately 15% .

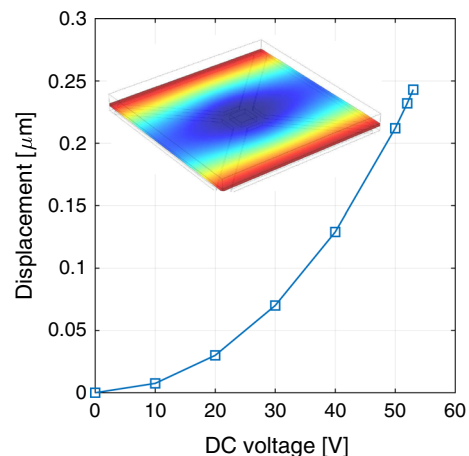


Fig. 4 FEM simulation of static displacement under different DC voltages

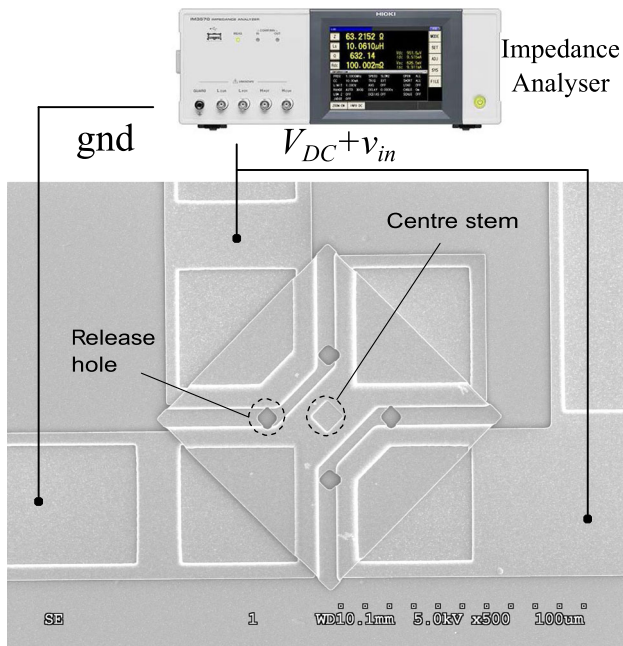


Fig. 5 SEM image of a single square plate resonator and its measurement setup

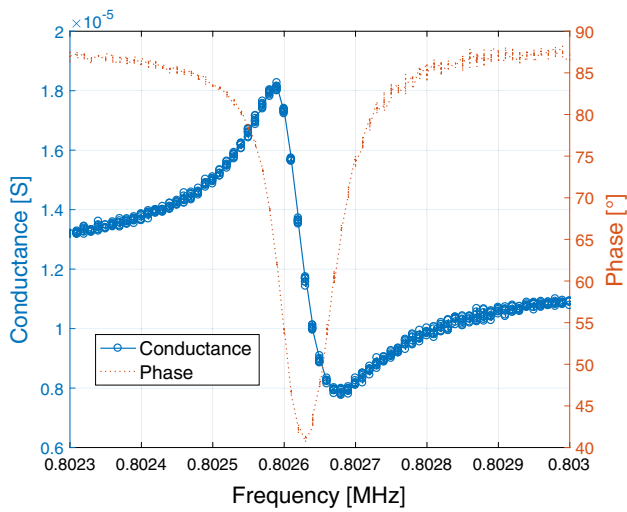


Fig. 6 Conductance and phase response of a single resonator

Damping effect has been characterized for a single resonator. The quality factor of the mechanical resonator can be estimated using the frequency to bandwidth ratio measured from the frequency spectrum

$$Q = \frac{f_0}{f_H - f_L} \tag{15}$$

where f_H and f_L are the high and low cut-off frequencies where the power is half the maximum value. The relation between the calculated quality factor Q and ambient pressure P is plotted in Fig. 7(a). The quality factor varies between 10 and 1.6×10^4 when the pressure drops from

3.6 kPa to 27 mPa. Figure 7(b) shows the square root of the electrostatic stiffness as a linear function of V_{DC} . The resonator collapses at a pull-in voltage about 25 V, which causes short circuit between the top plate and bottom electrodes, therefore burning the device. To prevent such irreversible process from happening and ensure good linearity, the recommended DC operating range is within 10 V, which allows a maximum 2.1% perturbation. The lower-than-expected pull-in voltage is attributed to the same over-sizing effect of the side length.

4 Coupled resonators array

Weakly coupled MEMS resonators demonstrate collective resonance behaviour at a unique set of eigen-modes that are different from a single resonator, and have been extensively explored as sensors with enhanced sensitivity, reduced connections and bandwidth, as well as the capability of multi-sensing. Coupling is first seen in micro cantilevers array, where the natural overhang structure introduces parasitic crosstalk between neighbouring elements.

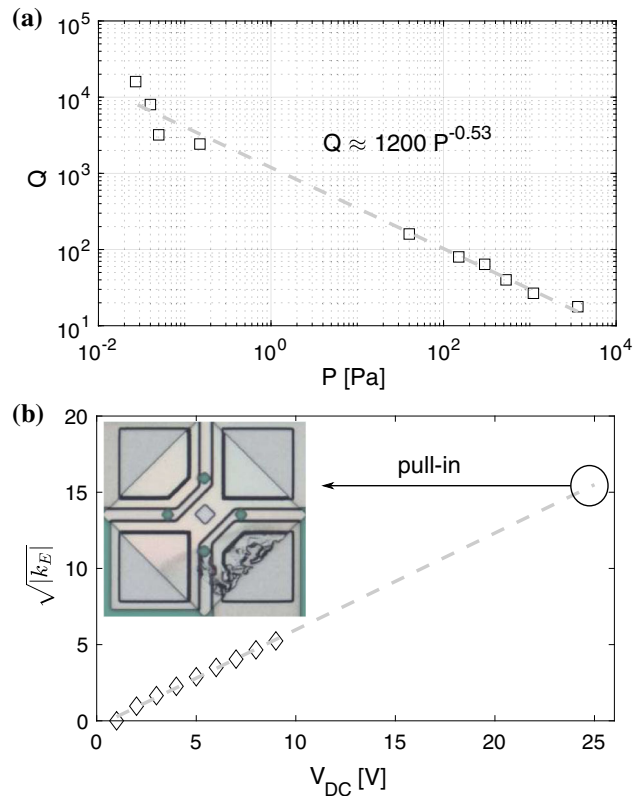


Fig. 7 Experimental characterization of a single resonator: **a** quality factor under different pressures and **b** square root of electrostatic stiffness as a linear function of DC bias voltage

To understand the coupling mechanism of the square plate resonators, Figure 8 presents the geometry of two adjacent plates. The two neighbouring membranes are coupled by arranging them in the same diagonal orientation and connecting two opposing corners using a mechanical beam that has a width W_C and a length L_C . The coupling beam is usually small hence providing a weak coupling ratio.

4.1 Eigen-mode analysis

Figure 9 reveals the eigen-modes of five corner coupled square plate resonators using COMSOL eigenfrequency analysis, along with the lumped-parameter spring mass model. Since all resonators are assumed to be identical, particular eigen-modes become too weak to be distinguished (e.g. the third resonator at the second and fourth mode) due to Anderson localisation [5]. In the presence of noise, a decrease in resonance amplitude would deteriorate the signal-to-noise ratio (SNR) and add complexity to subsequent signal processing. Hence for the conventional IEA method that applies a single actuation scheme by driving and reading out from one resonator, identifying all the eigenvalues of a large array can be challenging. However, one can drive and readout multiple resonators simultaneously to improve the power handling capability and increase the SNR.

4.2 Array configuration

The microscopic image of the designed five coupled array is shown in Fig. 10(a). A $20\ \mu\text{m} \times 10\ \mu\text{m}$ mechanical beam with the same Poly 2 material was used to couple the corners of two neighbouring square plates. Table 1 summarises the dimensions of the prototype MEMS resonators array. The interconnection wires have a designed width of $60\ \mu\text{m}$ and the entire sensor takes up a size of $920\ \mu\text{m} \times 330\ \mu\text{m}$.

To test the device, the ground electrodes of all five resonators were connected together. The first four elements (resonators 1–4) also shared the same DC supply, while the last element (resonator 5) was connected to an independent

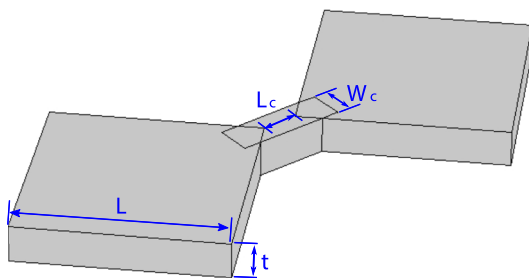


Fig. 8 Geometry of coupled square plate resonators

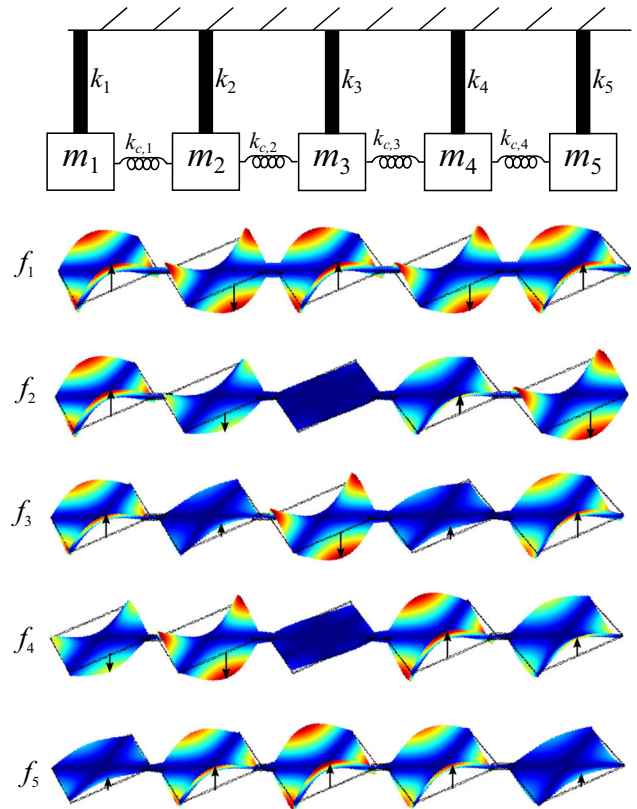


Fig. 9 Eigen-modes of five corner coupled square plate resonators and the spring mass model

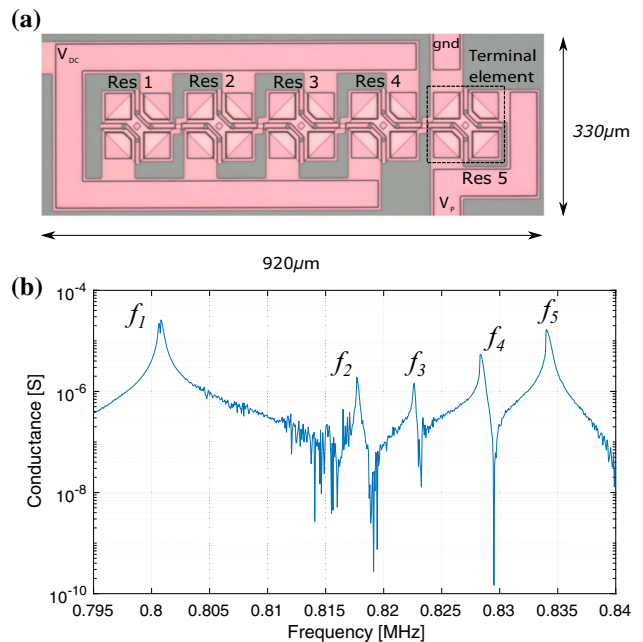


Fig. 10 a Microscopic image of the designed five coupled array and b its frequency response

bias voltage V_P to enable terminal perturbation. v_{in} was added to both V_{DC} and V_P and the current summation from

Table 1 Dimensions for the proposed corner coupled square plate MEMS resonators array

Parameter	Value	Unit
Plate side length, L	100	μm
Plate thickness, t	1.5	μm
Coupling beam length, L_C	20	μm
Coupling beam width, W_C	10	μm
Gap distance, g	0.75	μm

all elements was recorded. Figure 10(b) shows the five eigen-modes of frequency response. These eigenvalues can be used for subsequent perturbation analysis based on IEA, which will be discussed in the next section.

5 Sensor characterization

5.1 Perturbation analysis

Having determined all eigenvalues, perturbation can be performed by increasing the bias voltage of the terminal element V_p , which would introduce a negative electrostatic stiffness to such element. However, all the eigenvalues of the system would decrease due to collective coupling behaviour, and satisfy the following interweaving condition [10]:

$$\lambda_1^* < \lambda_1 < \lambda_2^* < \lambda_2 < \lambda_3^* < \lambda_3 < \lambda_4^* < \lambda_4 < \lambda_5^* < \lambda_5 \tag{16}$$

To validate this experimentally, V_p was changed from 0 to 10 V, while V_{DC} remained constant at 10 V. The frequency responses before and after perturbation are presented in Fig. 11. The eigen-frequencies shifted from 0.785, 0.822, 0.829, 0.837 and 0.847 MHz to 0.783, 0.819, 0.829, 0.835 and 0.845 MHz. λ and λ^* can therefore be calculated to extract the system matrix.

5.2 System matrix determination

Using the new IEA algorithm from Sect. 2, the system matrix (before perturbation) is determined to be

$$S = \begin{pmatrix} 2.68 & -0.13 & 0 & 0 & 0 \\ -0.13 & 2.57 & -0.13 & 0 & 0 \\ 0 & -0.13 & 2.68 & -0.05 & 0 \\ 0 & 0 & -0.05 & 2.76 & -0.02 \\ 0 & 0 & 0 & -0.02 & 2.72 \end{pmatrix} \times 10^{13} \tag{17}$$

with the perturbation amount being $\Delta S_{5,5} = -6 \times 10^{11}$, or 2.2% in terms of percentage. The result can be compared

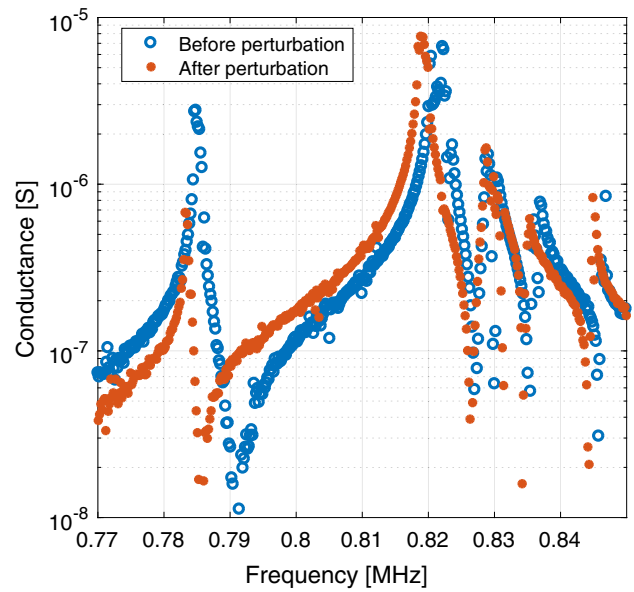


Fig. 11 Frequency response of five coupled array before and after terminal element perturbation

with the system matrix extracted from the previous Choubey’s deterministic approach

$$S = \begin{pmatrix} 2.71 & -0.13 & 0 & 0 & 0 \\ -0.13 & 2.57 & -0.13 & 0 & 0 \\ 0 & -0.13 & 2.67 & -0.05 & 0 \\ 0 & 0 & -0.05 & 2.75 & -0.02 \\ 0 & 0 & 0 & -0.02 & 2.72 \end{pmatrix} \times 10^{13} \tag{18}$$

The average discrepancy for diagonal and off-diagonal elements are 0.3 and 1.5% respectively, matching well with the prediction in Fig. 2.

5.3 Spring constant and coupling ratio

Sensor parameters such as mass, stiffness and coupling ratio can be derived from the extracted system matrix. The mass normalised spring constants of resonator 1–5 are $(2.55, 2.31, 2.51, 2.69, 2.70) \times 10^{13}$, which correspond to natural frequencies 0.804, 0.765, 0.797, 0.826 and 0.827 MHz. Hence the actual frequency variation of the PolyMUMPs fabrication is determined to be 3.2%.

The system matrix suggests a weak coupling varying from 0.8 to 4.9%, as these coupling springs are very small hence more prone to process error. Since the sensitivity of coupled resonators is highly dependent on the coupling ratio [20], it is important to optimise the design before using them as sensors. To understand how the geometry of these mechanical beams affects coupling ratio, resonators with different coupling beam lengths and widths can be

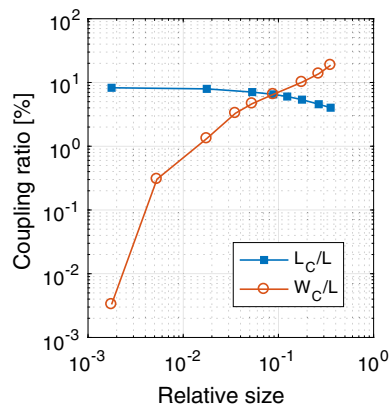


Fig. 12 Coupling ratios for various beam geometries

characterized with the IEA method. This can be done using a simple array of two coupled resonators in COMSOL. The coupling ratios for different beam geometries are derived and presented in Fig. 12 using the same perturbation analysis and IEA method. It can be seen that coupling strength is three orders of magnitude more sensitive to W_C than L_C . By changing the width alone, the coupling ratio is tunable from 0.003 to 20%.

6 Conclusion

We introduce a new inverse eigenvalue technique to investigate coupled micro/nano systems. With reduced algorithmic complexity and less than 1% system matrix error, the method has been experimentally verified using an example of five coupled square plate MEMS resonators with eigenfrequencies around 0.85 MHz. By obtaining two sets of eigenvalues before and after terminal perturbation, the IEA has been performed to derive the system matrix and hence important sensor and process information. The method offers improved accuracy and simplified readout, which can be used to actuate and characterize large array of coupled resonators, including ultrasound transducers and multi-function inertial sensors. As a proof of concept, only five resonators are examined in this paper. Theoretically, the maximum number of resonators in a coupled array is limited by the mode liaison effect, i.e. $n < \kappa Q \approx 100$ [20]. Hence we have fabricated larger arrays of twenty to fifty coupled resonators, which will be tested and used as sensors in our future work.

Acknowledgements We thank Ching-Mei Chen for designing the PCB. We acknowledge the help from Madhav Kumar in taking the SEM images. Authors would like to acknowledge the financial support by the European Commission, through FP7 Project iARTIST, Grant Agreement Nos. 611362, FP7-PEOPLE.

Open Access This article is distributed under the terms of the Creative Commons Attribution 4.0 International License (<http://creativecommons.org/licenses/by/4.0/>), which permits unrestricted use, distribution, and reproduction in any medium, provided you give appropriate credit to the original author(s) and the source, provide a link to the Creative Commons license, and indicate if changes were made.

References

- Chaste, J., Eichler, A., Moser, J., Ceballos, G., Rurali, R., & Bachtold, A. (2012). A nanomechanical mass sensor with yoctogram resolution. *Nature Nanotechnology*, 7(5), 301.
- Ghemari, Z., & Saad, S. (2017). Parameters improvement and suggestion of new design of capacitive accelerometer. *Analog Integrated Circuits and Signal Processing*, 92(3), 443.
- Mertz, J., Marti, O., & Mlynek, J. (1993). Regulation of a microcantilever response by force feedback. *Applied Physics Letters*, 62(19), 2344.
- Zhang, H., Li, B., Yuan, W., Kraft, M., & Chang, H. (2016). An acceleration sensing method based on the mode localization of weakly coupled resonators. *Journal of Microelectromechanical Systems*, 25(2), 286.
- Spletzer, M., Raman, A., Sumali, H., & Sullivan, J. P. (2008). Highly sensitive mass detection and identification using vibration localization in coupled microcantilever arrays. *Applied Physics Letters*, 92(11), 114102.
- de Lépinay, L. M., Pigeau, B., Besga, B., Vincent, P., Poncharal, P., & Arcizet, O. (2016). A universal and ultrasensitive vectorial nanomechanical sensor for imaging 2D force fields. *Nature Nanotechnology*, 12, 156.
- Jackson, S., Gutschmidt, S., Roeser, D., & Sattel, T. (2017). Development of a mathematical model and analytical solution of a coupled two-beam array with nonlinear tip forces for application to AFM. *Nonlinear Dynamics*, 87(2), 775.
- Zhang, H., Chang, H., & Yuan, W. (2017). Characterization of forced localization of disordered weakly coupled micromechanical resonators. *Microsystems & Nanoengineering*, 3, 17023.
- DeMartini, B. E., Rhoads, J. F., Zielke, M. A., Owen, K. G., Shaw, S. W., & Turner, K. L. (2008). A single input-single output coupled microresonator array for the detection and identification of multiple analytes. *Applied Physics Letters*, 93(5), 054102.
- Choubey, B., Boyd, E. J., Armstrong, I., & Uttamchandani, D. (2012). Determination of the anisotropy of Young's modulus using a coupled microcantilever array. *Journal of Microelectromechanical Systems*, 21(5), 1252.
- Tao, G., & Choubey, B. In *2017 IEEE 12th international conference on nano/micro engineered and molecular systems (NEMS)*, pp. 657–660. IEEE
- Tao, G., & Choubey, B. (2016). A simple technique to readout and characterize coupled MEMS resonators. *Journal of Microelectromechanical Systems*, 25(4), 617.
- Choubey, B., Anthony, C., Saad, N. H., Ward, M., Turnbull, R., & Collins, S. (2010). Characterization of coupled micro/nanoresonators using inverse eigenvalue analysis. *Applied Physics Letters*, 97(13), 133114.
- Lanczos, C. (1950). An iteration method for the solution of the eigenvalue problem of linear differential and integral operators. *Journal of Research of the National Bureau of Standards*, 45(4), 255–282.
- Tao, G., Choubey, B. (2016). In *Journal of physics: conference series* (Vol. 757, p. 012017). IOP Publishing.
- Demirci, M. U., & Nguyen, C. T. C. (2006). Mechanically corner-coupled square microresonator array for reduced series

motional resistance. *Journal of Microelectromechanical Systems*, 15(6), 1419.

17. Koester, D., Cowen, A., Mahadevan, R., Stonefield, M., & Hardy, B. (2003). *PolyMUMPs design handbook*. Durham: MEMSCAP Inc.
18. Weaver, W. Jr., Timoshenko, S. P., & Young, D. H. (1990). *Vibration problems in engineering*. Hoboken: Wiley.
19. Ladabaum, I., Jin, X., Soh, H. T., Atalar, A., & Khuri-Yakub, B. (1998). Surface micromachined capacitive ultrasonic transducers. *IEEE Transactions on Ultrasonics, Ferroelectrics, and Frequency Control*, 45(3), 678.
20. Thiruvengatanathan, P., Woodhouse, J., Yan, J., & Seshia, A. A. (2011). Limits to mode-localized sensing using micro-and nanomechanical resonator arrays. *Journal of Applied Physics*, 109(10), 104903.



Guowei Tao received the B.Sc. degree from Fudan University, and the B.Eng. degree (Hons.) from the University of Birmingham. He is currently pursuing the D.Phil. degree with the Microelectronic Circuits and Analogue Devices Research Group, Department of Engineering Science, University of Oxford. He has received a number of awards including the Marie Curie Fellowship, China Oxford Scholarship Fund and Santander Scholarship. His

research interests include M/NEMS array, coupled resonators,

perturbation analysis, process and device characterization, and ultrasound transducers.



Bhaskar Choubey received the D.Phil. degree from the University of Oxford as a Rhodes Scholar, and the B.Tech. degree from the Regional Engineering College, Warangal, India. He is currently an Associate Professor of Engineering Science and a Fellow with Somerville College, University of Oxford, UK. He has been at the University of Glasgow, the Max Planck Institute of Brain Research and North West University, South

Africa. His research interests include CMOS image sensor, nonlinear dynamics, human visual system, and microelectromechanical systems. He received the IEEE Sensors Council GOLD Early Career Achievement Award, and the Myril B. Reed Best Paper Award from the IEEE Midwest Symposium of Circuits and Systems. He has served as an Associate Editor of the IEEE Transactions on Circuits and Systems II and the IEEE Sensors Journal.